

Articles

New Open-Framework Nonlinear Optical Materials. Crystal Structure of $\text{Na}_{1/2}(\text{H}_3\text{O})_{1/2}\text{Nb}_2\text{PO}_8$ and Physical Properties of the Solid Solution $\text{K}_{2/3}\text{Li}_{1/3}\text{Nb}_{2-x}\text{Ta}_x\text{PO}_8$

Cheryl S. Liang,[†] William T. A. Harrison,^{*‡} Michael M. Eddy,^{†,§}
Thurman E. Gier,[†] and Galen D. Stucky^{*†}

Department of Chemistry, University of California, Santa Barbara, California 93106-9510, and
Department of Chemistry, University of Houston, Houston, Texas 77204-5641

Received April 20, 1992. Revised Manuscript Received April 19, 1993

The syntheses, structures, and physical properties of several members of a new family of noncentrosymmetric, open-framework, ion-exchangeable phases which have a substantial nonlinear optical response (Nd:YAG 1064 nm) are described. Single-crystal (to 2 mm) hydrothermal synthesis of $\text{Na}_{1/2}(\text{H}_3\text{O})_{1/2}\text{Nb}_2\text{PO}_8$ was carried out at 30 000–40 000 psi and 650–700 °C. The structure of $\text{Na}_{1/2}(\text{H}_3\text{O})_{1/2}\text{Nb}_2\text{PO}_8$, as determined from single-crystal X-ray data consists of an octahedral (NbO_6)/tetrahedral (PO_4) framework, connected *via* Nb–O–P and Nb–O–Nb bonds, with cavities and channels occupied by the Na^+ and H_3O^+ cations. Members of the solid solution $\text{K}_{2/3}\text{Li}_{1/3}\text{Nb}_{2-x}\text{Ta}_x\text{PO}_8$ ($0 < x < 2$) have been synthesized as powders by solid-state methods and are all isomorphous with $\text{Na}_{1/2}(\text{H}_3\text{O})_{1/2}\text{Nb}_2\text{PO}_8$. Various ion-exchange reactions with NH_4^+ , Rb^+ , and Ag^+ are possible. These materials have been characterized by X-ray powder diffraction, TGA, ^{31}P MAS NMR spectroscopy, second-harmonic generation measurements, and UV/visible spectroscopy. Crystal data: $\text{Na}_{1/2}(\text{H}_3\text{O})_{1/2}\text{Nb}_2\text{PO}_8$, $M_r = 364.94$, rhombohedral, $R32$ (No. 155), $a = 8.4962(5)$ Å, $\alpha = 104.775(2)^\circ$, $V = 538.77$ Å³, $Z = 3$, $R = 2.88\%$, $R_w = 3.56\%$ for 66 parameters and 743 observations [$I > 3\sigma(I)$].

Introduction

The potassium titanyl phosphate (KTiOPO_4 ; hereafter KTP) family of phases are currently the subject of great interest due to their technologically important nonlinear and electrooptical properties.^{1,2} A wide variety of complete or partial substitutions are possible for the octahedral (Ti), tetrahedral (P), and cation (K) sites in KTP, while maintaining the KTP-type orthorhombic structure.² Potassium cations in the KTP structure can be easily ion exchanged, and in fact, small molecule (NH_3 , H_2O) gas-phase adsorption/desorption reactions are also possible with the maintenance of crystal optical quality.³ The effect of the guest cation on optical behavior has been shown to be profound^{4,5} and is a crucial factor in the synthesis of waveguide materials.⁶ In general, zeolite-like host/guest structures with electrooptic active frameworks provide an excellent opportunity for the dynamic control of optical response by ion-exchange methods.

Our interest in preparing new types of materials with large SHG responses has led us to a search for tantalum/niobium-containing inclusion compounds which can be ion exchanged. Here, we report the syntheses and characterization of several structural members of a new three-dimensional, anionic, octahedral/tetrahedral open framework. The structure of hydrothermally grown $\text{Na}_{1/2}(\text{H}_3\text{O})_{1/2}\text{Nb}_2\text{PO}_8$ has been solved from X-ray single crystal data. The complete Nb/Ta solid solution $\text{K}_{2/3}\text{Li}_{1/3}\text{Nb}_{2-x}\text{Ta}_x\text{PO}_8$ (analogues of $\text{Na}_{1/2}(\text{H}_3\text{O})_{1/2}\text{Nb}_2\text{PO}_8$) has been prepared and characterized by crystallographic, ^{31}P MAS NMR, SHG, vis/UV, and ion-exchange measurements. The relationship between crystal structure, SHG behavior, and spectroscopic properties is briefly discussed for this family of compounds.

Experimental Section

Single-Crystal Growth. High-temperature/high-pressure hydrothermal methods were utilized: $\text{Na}_{1/2}(\text{H}_3\text{O})_{1/2}\text{Nb}_2\text{PO}_8$ crystals were prepared from a mixture of $\text{NaH}_2\text{PO}_4 \cdot \text{H}_2\text{O}$ (Fisher, reagent grade), $\text{Na}_2\text{HPO}_4 \cdot 7\text{H}_2\text{O}$ (Fisher, reagent grade), Nb_2O_5 , and H_2O , which was sealed in a gold ampule and heated at 650 °C (estimated pressure 45 000 psi) for 20 h in a Leco Tem-Press hydrothermal bomb. The tube was slow-cooled at 8 °C/h to 400 °C and cooled to room temperature overnight. Many transparent, rodlike crystals with a maximum linear dimension of ~2 mm were recovered by washing in water, then filtered, and air dried. Single crystals of $\text{Na}_{1-x}(\text{H}_3\text{O})_x\text{Ta}_2\text{PO}_8$ were grown from a mixture of $\text{NaH}_2\text{PO}_4 \cdot \text{H}_2\text{O}$ (10 mmol), Ta_2O_5 (0.4 mmol), and H_2O , which was sealed in a gold tube and heated to 700 °C (~32 000 psi) for 60 h, then cooled at 8 °C/h to 400 °C, and quenched to ambient.

[†] University of California.

[‡] University of Houston.

[§] Present address: Superconductor Technologies Inc., 460 Ward Drive, Goleta, CA 93117.

(1) Bierlein, J. D.; Vanherzeele, H. *J. Opt. Soc. Am.* 1989, **B6**, 622.

(2) Stucky, G. D.; Phillips, M. L. F.; Gier, T. E. *Chem. Mater.* 1989, **1**, 492.

(3) Eddy, M. M.; Gier, T. E.; Keder, N. L.; Stucky, G. D.; Cox, D. E.; Bierlein, J. D.; Jones, G. *Inorg. Chem.* 1988, **27**, 1856.

(4) Phillips, M. L. F.; Harrison, W. T. A.; Gier, T. E.; Stucky, G. D. *Proc. SPIE* 1989, **1104**, 225.

(5) Phillips, M. L. F.; Harrison, W. T. A.; Stucky, G. D.; McCarron III, E. M.; Calabrese, J. C.; Gier, T. E. *Chem. Mater.* 1992, **4**, 222.

(6) Risk, W. P. *Appl. Phys. Lett.* 1991, **58**, 19.

Many tiny transparent crystals (dimension $\sim 20 \mu\text{m}$) were produced. Solid-state preparations of the phases "NaNb₂PO₈" or "NaTa₂PO₈" were unsuccessful, resulting in other, unidentified phases, and the sodium-containing phases in this family of materials can be directly prepared only *via* hydrothermal methods.

Solid-State Synthesis. Members of the K_{2/3}Li_{1/3}Nb_{2-x}Ta_xPO₈ solid solution, with $x = 0.00, 0.25, 0.33, 0.50, 0.75, 1.00, 1.25, 1.50, 1.67, 1.75,$ and $2.00,$ were synthesized by standard solid-state methods. Stoichiometric amounts of KHCO₃ (MCB, reagent grade), Li₂CO₃ (Fisher, reagent grade, predried at 500 °C for 20 h), Nb₂O₅ (Aldrich, 99.99%), Ta₂O₅ (Johnson-Matthey, Grade "1"), and NH₄H₂PO₄ (Fisher, reagent grade) were thoroughly mixed in a mechanical grinder, placed in a Pt crucible, and slowly heated in a muffle furnace to 350 °C to drive off H₂O, CO₂, and NH₄OH, followed by an anneal at 750 °C. Each mixture was removed from the furnace, thoroughly ground, and fired at 1000 °C for 15 h and subsequently quenched on an aluminum plate to room temperature. An off-white powder resulted for each reaction.

Members of the solid-solution Rb_{2/3}Li_{1/3}Nb_{2-x}Ta_xPO₈ were synthesized using the same method as for the K_{2/3}Li_{1/3}Nb_{2-x}Ta_xPO₈ series, by substituting a stoichiometric amount of rubidium (50% RbOH solution from Strem Chemicals) for the potassium-containing precursor. The mixture was heated in a muffle furnace to 150 °C for 1 h to evaporate water, then the temperature was slowly increased to 750 °C to drive off additional H₂O, CO₂, and NH₄OH. After thorough grinding, the final firing temperature was 1000 °C.

For all phases, X-ray powder diffraction data were collected on a Scintag PAD-X θ - θ powder diffractometer using Cu K α radiation ($\lambda = 1.54178 \text{ \AA}$). The patterns were indexed using single-crystal unit cell lattice constants of Na_{1/2}(H₃O)_{1/2}Nb₂PO₈, and the lattice parameters were refined using Scintag software.

Ion-Exchange Reactions. Na_{2/3}Li_{1/3}Nb₂PO₈ was prepared by treating 0.5 g of polycrystalline K_{2/3}Li_{1/3}Nb₂PO₈ with 2.0 g of NaNO₃ (Fisher, reagent grade). The mixture was heated to 320 °C for 3 days in a Pt crucible, and the white-powder product was recovered by washing the melt with water, followed by filtration. (NH₄)_{2/3}Li_{1/3}Nb₂PO₈ was prepared as follows: A flux of 1.601 g of NH₄NO₃ (Fisher, reagent grade) and 0.454 g (5 mol %) Ba(NO₃)₂ (Fisher, reagent grade) were mixed with 0.500 g of K_{2/3}Li_{1/3}Nb₂PO₈ and heated in a covered vessel for 4 days at 200 °C. The melt was cooled and dissolved in hot water and subsequently filtered, rinsed with methanol, and air dried, resulting in a white powder. K_{2/3}Ag_{1/3}Nb₂PO₈ was prepared by mixing 0.5 g of K_{2/3}Li_{1/3}Nb₂PO₈ with 2.0 g of AgNO₃ (Fisher, reagent grade) and heating for 2 days at 230 °C. Soluble byproducts from the melt were dissolved in hot water and the product recovered by filtration. The filtrate was tested with dilute HCl for the presence of Ag⁺. This phase slowly darkens when exposed to light and also appears to be sensitive to X-radiation.

Characterization was by X-ray powder diffraction, weight uptake or loss, and ³¹P MAS NMR spectroscopy, as described below.

Structure Determination. A suitable single crystal of Na_{1/2}(H₃O)_{1/2}Nb₂PO₈, of approximate dimensions 0.2 × 0.2 × 0.2 mm, was selected for structure determination and mounted on a thin glass fiber with epoxy resin. Room temperature [25(2) °C] intensity data were collected on a Huber automated 4-circle diffractometer (graphite-monochromated Mo K α radiation, $\lambda = 0.71073 \text{ \AA}$) as outlined in Table I. Initially, 25 reflections were located and centered by searching reciprocal space ($10^\circ < 2\theta < 25^\circ$) and indexed to obtain a unit cell and orientation matrix. The lattice parameters were optimized by least-squares refinement, resulting in rhombohedral cell constants of $a = 8.4962(5) \text{ \AA}$ and $\alpha = 104.775(2)^\circ$ (digits in parentheses = esd's). Intensity data were collected in the θ - 2θ scanning mode for $0 < 2\theta < 65^\circ$ with three standard reflections monitored/100 observations for intensity variation throughout the course of the experiment. The scan speed was 6°/min with a scan range of 1.3° below K α_1 to 1.6° above K α_2 . No significant variation in standards was observed, and crystal absorption, which was minimal, was empirically corrected for by using ψ scans through 360° for selected reflections with $\chi \sim 90^\circ$. The raw intensities were

Table I. Crystallographic Parameters for Na_{1/2}(H₃O)_{1/2}Nb₂PO₈

empirical formula	Nb ₂ PNa _{0.5} O _{8.5} H _{0.667}
mol wt	364.94
habit	colorless rhomb
crystal system	trigonal
$a = b = c$ (Å)	8.4962(5)
$\alpha = \beta = \gamma$ (deg)	104.775(2)
V (Å ³)	538.77
Z	3
space group	R32 (No. 155)
T (°C)	25(2)
λ (Mo K α) (Å)	0.71073
ρ_{calc} (g/cm ³)	3.374
μ (Mo K α) (cm ⁻¹)	33.2
absorption correction	ψ scan
hkl data limits	$-10 \leq h, -10 \leq k, 10 \leq l$
reflections collected	818
observed data ^a	743
parameters	66
$R(F_o)^b$ (%)	2.88
$R_w(F_o)^c$ (%)	3.56

^a $I > 3\sigma(I)$ after merging, as described in text. ^b $R = \sum ||F_o| - |F_c|| / \sum |F_o|$. ^c $R_w = [\sum w(|F_o| - |F_c|)^2 / \sum w|F_o|^2]^{1/2}$.

reduced to F and $\sigma(F)$ values using a Lehmann-Larson profile-fitting routine,⁷ and the normal corrections for Lorentz and polarization effects were made. All the data collection and reduction routines were based on the UCLA crystallographic computing package.⁸ There were no systematic absences apparent in the reduced data, consistent with five distinct trigonal space groups: $R3, R\bar{3}, R32, R3m,$ and $R\bar{3}m$. The powder second-harmonic-generation (PSHG) response⁹ of Na_{1/2}(H₃O)_{1/2}Nb₂PO₈ was nonzero, eliminating the centrosymmetric space groups ($R\bar{3}$ and $R\bar{3}m$), and consideration of Laue equivalences indicated that the space group was $R32$ or $R3m$. 818 reflections were measured, of which 746 were used in the structure solution and refinement [merging $R = 5.4\%$; reflections with $I < 3\sigma(I)$ considered unobserved]. Some Friedel equivalences were not merged during this process, in order to determine the absolute configuration of the structure during the refinement, by the Flack procedure.¹⁰

The structure of Na_{1/2}(H₃O)_{1/2}Nb₂PO₈ was solved by a combination of direct methods and Fourier syntheses, assuming the space group was noncentrosymmetric $R32$ (No. 155), as confirmed by the course of the subsequent refinement. Conversely, no reasonable starting model could be obtained in space group $R3m$. A direct-methods solution for the heavy atoms of the framework was obtained from the program SHELXS-86¹¹ and the oxygen and sodium atoms were located from Fourier difference maps following refinement of the known atom positions. Partial site occupancies were assigned to some of the atoms, as described below. The least-squares, Fourier, and subsidiary calculations were performed using the Oxford CRYSTALS¹² system, running on a DEC Micro VAX-II computer. Final full-matrix refinements were against F and included anisotropic temperature factors and a Larson isotropic secondary extinction correction,¹³ which refined to 67(6). The Flack polarity parameter¹⁰ was included in the last cycles of refinement [refined value = $-0.04(2)$] and the polarity of the structure is as set out below. Neutral-atom scattering factors, taking account of anomalous dispersion terms, were obtained from *International Tables*.¹⁴ Final residuals, defined in Table I, of $R(F) = 2.88\%$ and $R_w(F) = 3.56\%$ ($w_i = 1$) were

(7) Lehmann, M. S.; Larsen, F. K. *Acta Crystallogr.* 1974, **A30**, 580.

(8) Locally modified version of the UCLA Crystallographic Computing Package, developed by C.E. Strouse, Department of Chemistry, UCLA, Los Angeles, CA.

(9) Dougherty, J. P.; Kurtz, S. K. *J. Appl. Crystallogr.* 1976, **9**, 145.

(10) Flack, H. D. *Acta Crystallogr.* 1983, **A39**, 876.

(11) Sheldrick, G. M. SHELXS-86 User Guide, Crystallography Department, University of Göttingen, Germany, 1986.

(12) Watkin, D. J.; Carruthers, J. R.; Betteridge, P. W. CRYSTALS User Guide, Chemical Crystallography Laboratory, Oxford University, UK, 1990.

(13) Larson, A. C. In *Crystallographic Computing*; Ahmed, F. R., Ed.; Munksgaard: Copenhagen, 1970; p 291.

(14) Cromer, D. T. *International Tables for X-Ray Crystallography*; Kynock Press: Birmingham, 1974; Volume IV, Table 2.3.1.

obtained. Final Fourier difference maps revealed no regions of electron density which could be assigned to additional atomic sites (min = -0.6 , max = $1.7 \text{ e } \text{\AA}^{-3}$), and analysis of the various trends in F_o versus F_c revealed no unusual effects. As a final check on the crystal symmetry, the refined atomic coordinates of $\text{Na}_{1/2}(\text{H}_3\text{O})_{1/2}\text{Nb}_2\text{PO}_8$ were processed by the program MISSYM,¹⁵ which checks a crystal model for "missing" or extra symmetry elements. No additional symmetry to that already present in space group $R32$ could be found, even upon allowing the atoms to shift by up to 0.75 \AA from their experimentally determined positions. Thus it appears that $\text{Na}_{1/2}(\text{H}_3\text{O})_{1/2}\text{Nb}_2\text{PO}_8$ does not transform by a displacive-type transition to a centrosymmetric structure at elevated temperatures, as do the KTP family of phases,¹⁶ and many perovskite structures which show interesting optical properties.¹⁷ Tables of observed and calculated structure factors are available as supplementary material (see paragraph at end of paper).

Optical, Spectroscopic, and Thermal Measurements. Second harmonic generation (SHG) efficiencies relative to α -quartz were measured on an apparatus similar to that described by Dougherty and Kurtz⁹ in reflection mode. A Q-switched pulsed Nd:YAG laser operating at 1064 nm was used as the radiation source. Appropriate precautions to filter spurious light were taken. The samples were loaded in capillaries of 1-mm inner diameter and sealed. A total of 10 measurements/sample were made, each measurement averaged over 20 traces, using single-shot mode with pulses fired at a 2-Hz interval between traces. All SHG intensities were measured and referenced the same way as the quartz standard.

Vis/UV spectra, using MgCO_3 as a standard, were obtained using an automated Cary 14 Vis/UV spectrometer operating in the wavelength range $220\text{--}850 \text{ nm}$. The absorption edge reported is the inflection point of the absorption profile. IR data were collected on a Biorad FTS-60 FTIR spectrometer using a diffuse-reflectance apparatus supplied by Spectra Tech Inc., and a Kubelka-Munk function was applied to all spectra. Thermogravimetric analysis (TGA) measurements were carried out on a du Pont 9900 TGA/DSC system. The samples were placed on platinum sample holders, and all samples were ramped at $10 \text{ }^\circ\text{C}/\text{min}$ from 50 to $900 \text{ }^\circ\text{C}$.

Solid-state ^{31}P MAS NMR spectra were obtained on a General Electric GN-300 wide-bore system operating at 121.65 MHz , equipped with a high-power Chemagnetics magic angle spinning probe. Samples were loaded in 9.5-mm -outside-diameter Kel-F spinners and spun at speeds between 3.2 and 3.5 kHz . Standard single-pulse acquisition was utilized with a $7\text{-}\mu\text{s}$, 90° pulse length, and recycle delays of 10 s . All samples were referenced to external $85\% \text{ H}_3\text{PO}_4$ (downfield shifts defined as positive). An inversion recovery (TI-IR) experiment (pulse sequence $180^\circ\text{--}\tau\text{--}90^\circ$) was carried out for the determination of phase purity in $\text{K}_2/3\text{-Li}_{1/3}\text{Ta}_2\text{PO}_8$ with a 7.5-ms , 90° pulse length, recycle delay of 60 s , and dwell times (τ) of 10 ms , 100 ms , 300 ms , 500 ms , 1 s , 3 s , 5 s , 10 s , 20 s , 60 s , 120 s , 300 s , 600 s , and 900 s .

Results

Crystal Structure. The final atomic positional and equivalent thermal parameters for $\text{Na}_{1/2}(\text{H}_3\text{O})_{1/2}\text{Nb}_2\text{PO}_8$ are given in Table II, with selected geometrical data in Table III. The asymmetric unit of $\text{Na}_{1/2}(\text{H}_3\text{O})_{1/2}\text{Nb}_2\text{PO}_8$ consists of 10 atoms—3 "guest" cations (two sodium cations and one hydronium (H_3O^+) ion), whose coordination is discussed below, and 7 "framework" species, consisting of a niobium atom (octahedral oxygen coordination), a phosphorus atom (tetrahedral) and 5 oxygen atoms which make either Nb–O–Nb or Nb–O–P bridges. Some of these O atoms also bond to the guest species, as described later.

Table II. Atomic Positional Parameters for $\text{Na}_{1/2}(\text{H}_3\text{O})_{1/2}\text{Nb}_2\text{PO}_8$

atom	W^a	x	y	z	$U_{eq}(\text{\AA}^2)^b$	frac ^c
Nb(1)	6f	0.96222(7)	0.84856(7)	0.64672(7)	0.0086	
P(1)	3e	1/2	0.2688(2)	0.7312	0.0076	
O(1)	6f	0.7669(6)	0.6387(6)	0.4436(6)	0.0112	
O(2)	6f	0.1284(6)	0.7175(6)	0.5816(6)	0.0111	
O(3)	6f	0.7899(6)	0.9279(6)	0.6879(6)	0.0109	
O(4)	3e	1/2	0.0237(5)	0.9763	0.0126	
O(5)	3d	0	0.8486(5)	0.1514	0.0129	
Na(1)	1b	1/2	1/2	1/2	0.0222	1.0
Na(2)	3d	0	0.421(2)	0.579	0.0128	0.168(5)
O(6) ^c	3e	1/2	0.790(2)	0.210	0.0506	0.498(5)

^a Wyckoff letter. ^b $U_{eq} = (U_1U_2U_3)^{1/3}$. ^c Fractional site occupancy. ^d Hydronium ion oxygen atom.

Table III. Selected Bond Distances (\AA) and Angles (deg) for $\text{Na}_{1/2}(\text{H}_3\text{O})_{1/2}\text{Nb}_2\text{PO}_8$

Nb(1)–O(1)	2.091(4)	Nb(1)–O(2)	2.102(5)
Nb(1)–O(3)	1.834(5)	Nb(1)–O(3)'	2.062(5)
Nb(1)–O(4)	1.933(3)	Nb(1)–O(5)	1.896(3)
P(1)–O(1)	1.543(5) $\times 2$	P(1)–O(2)	1.520(5) $\times 2$
Na(1)–O(1)	2.498(5) $\times 6$	Na(2)–O(2)	2.47(2) $\times 2$
Na(2)–O(3)	2.815(6) $\times 2$	Na(2)–O(6) ^a	2.00(2)
O(6)–O(1)	3.35(2) $\times 2$	O(6)–O(2)	2.95(1) $\times 2$
O(6)–O(3)	3.20(2) $\times 2$	O(6)–O(4)	3.15(3) $\times 2$
O(2)–Nb(1)–O(1)	84.6(2)	O(3)–Nb(1)–O(1)	87.0(2)
O(3)–Nb(1)–O(2)	170.7(2)	O(3)–Nb(1)–O(1)	84.1(2)
O(3)–Nb(1)–O(2)	83.2(2)	O(3)–Nb(1)–O(3)	92.0(3)
O(4)–Nb(1)–O(1)	94.8(2)	O(4)–Nb(1)–O(2)	85.8(2)
O(4)–Nb(1)–O(3)	98.9(2)	O(4)–Nb(1)–O(3)	169.0(2)
O(5)–Nb(1)–O(1)	167.3(2)	O(5)–Nb(1)–O(2)	87.7(1)
O(5)–Nb(1)–O(3)	99.8(2)	O(5)–Nb(1)–O(3)	85.0(2)
O(5)–Nb(1)–O(4)	94.7(1)		
O(1)–P(1)–O(1)	105.4(4)	O(2)–P(1)–O(1)	109.3(3) $\times 2$
O(2)–P(1)–O(1)	110.5(3) $\times 2$	O(2)–P(1)–O(2)	111.7(4)
P(1)–O(1)–Nb(1)	143.0(3)	P(1)–O(2)–Nb(1)	140.7(3)
Nb(1)–O(3)–Nb(1)	145.9(3)	Nb(1)–O(4)–Nb(1)	153.3(4)
Nb(1)–O(5)–Nb(1)	174.8(5)		

^a Apparent contact due to partial site occupancies.

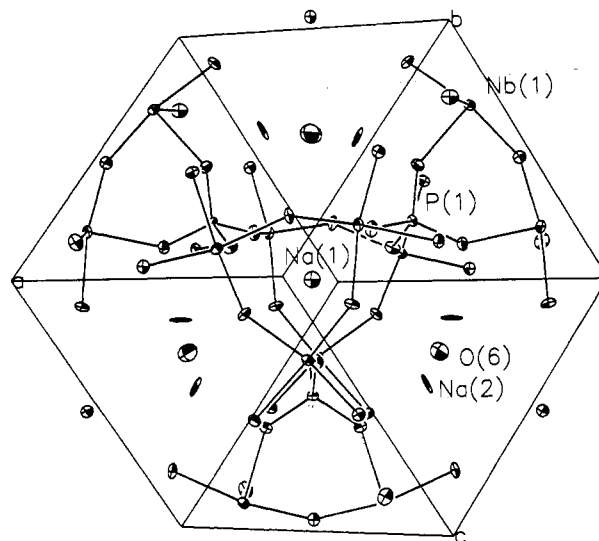


Figure 1. ORTEP diagram of the crystal structure of $\text{Na}_{1/2}(\text{H}_3\text{O})_{1/2}\text{Nb}_2\text{PO}_8$, viewed down the $[111]$ direction. 50% thermal ellipsoids, with selected atoms labelled.

The crystal structure of $\text{Na}_{1/2}(\text{H}_3\text{O})_{1/2}\text{Nb}_2\text{PO}_8$ is illustrated in Figures 1 and 2.

$\text{Na}_{1/2}(\text{H}_3\text{O})_{1/2}\text{Nb}_2\text{PO}_8$ adopts a new crystal structure, consisting of a three-dimensional array of vertex-sharing NbO_6 octahedra and PO_4 tetrahedra, enclosing a network of cavities, where the sodium and hydronium cations reside. The cavities are connected through one-dimensional channels, aligned in the rhombohedral $[111]$ direction,

(15) Le Page, Y. J. *Appl. Crystallogr.* 1988, 21, 983.

(16) Harrison, W. T. A.; Gier, T. E.; Stucky, G. D.; Schultz, A. J. *Chem. Commun.* 1990, 540.

(17) Galasso, F. S. *Structure, Properties and Preparation of Perovskite-Type Compounds*; Pergamon Press: Oxford, 1969.

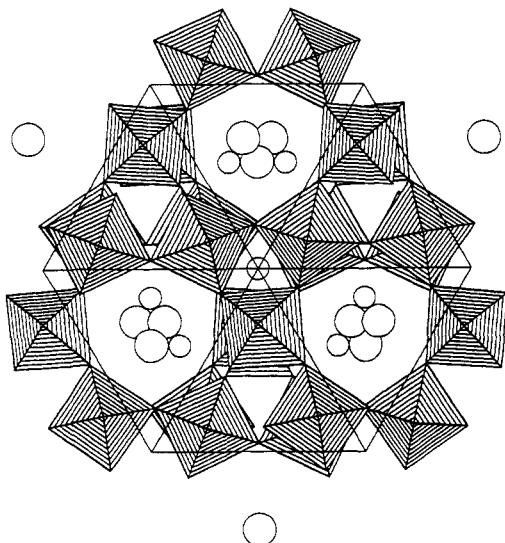


Figure 2. Polyhedral (STRUPLO) diagram of the octahedral/tetrahedral framework in $\text{Na}_{1/2}(\text{H}_3\text{O})_{1/2}\text{Nb}_2\text{PO}_8$, viewed down the [111] direction, showing the one-dimensional channel system, and extra-framework atoms. The disordered guest O(6) species are indicated by large circles, Na species by small circles.

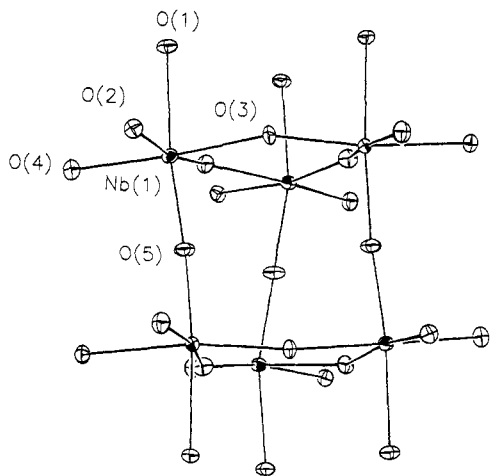


Figure 3. Detail of the crystal structure of $\text{Na}_{1/2}(\text{H}_3\text{O})_{1/2}\text{Nb}_2\text{PO}_8$, showing the Nb_6O_{27} 6-octahedron unit. 50% thermal ellipsoids.

via 6-ring windows, surrounded by NbO_6 units. The building block of the structure may be viewed as 6 niobium/oxygen octahedra linked into a Nb_6O_{27} trigonal prism (Figure 3), centered at the point (0,0,0). Of the oxygen atoms, O(3) forms the Nb–O–Nb links at the ends of the prism, while three almost linear Nb(1)–O(5)–Nb(1) bonds [$\theta = 174.6(5)^\circ$] link the two ends of the prism. Of the other three vertices around each Nb atom, two oxygen atoms [O(1) and O(2)] are involved in Nb–O–P bonds, and the remaining oxygen atom, O(4), links the Nb_6 -centered prisms via Nb–O–Nb bonds into trigonal layers with an ABC repeating motif. Each PO_4 tetrahedron (site symmetry 0.2, $d_{\text{av}}(\text{P–O}) = 1.533(3) \text{ \AA}$) makes four P–O–Nb links to four distinct Nb_6O_{27} units. Two of these P–O–Nb bonds are to niobium atoms in the same layer, one P–O–Nb link is to a Nb_6O_{27} prism above the phosphorus atom, and the other vertex is to a similar group below.

The NbO_6 octahedron in $\text{Na}_{1/2}(\text{H}_3\text{O})_{1/2}\text{Nb}_2\text{PO}_8$ is distorted, with bond lengths varying from 1.834(5) Å to 2.102(5) Å ($d_{\text{av}}(\text{Nb–O}) = 1.987(2) \text{ \AA}$). The *cis* O–Nb–O bond angles vary from 83.2(2)° to 99.8(2)°. The cation octa-

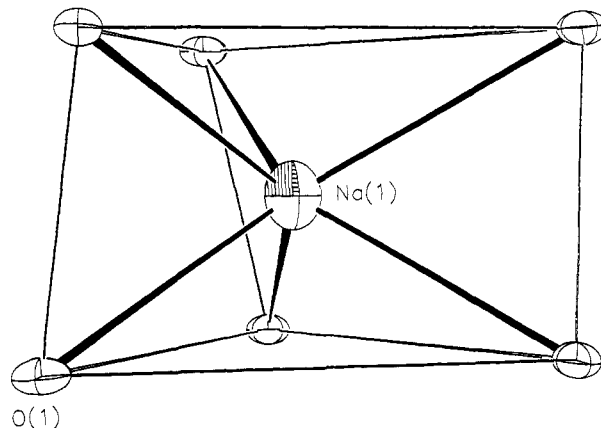


Figure 4. Na(1) coordination in $\text{Na}_{1/2}(\text{H}_3\text{O})_{1/2}\text{Nb}_2\text{PO}_8$ showing its almost trigonal prismatic coordination geometry with respect to its six equivalent O(1) neighbors.

hedral displacement, defined as

$$\Delta_{\text{Oct}} = r(\text{Nb}) - \frac{1}{6} \sum r(\text{O})$$

where r are orthogonal atomic coordinates, and the summation is over the six octahedral nearest-neighbor oxygen atoms, of the NbO_6 group gives $\Delta_{\text{Oct}} = 0.203 \text{ \AA}$. Notably, this distortion is not along an Nb–O bond axis, as typically found in tetragonally distorted perovskite phases such as KNbO_3 , but rather, the Nb atom in the NbO_6 group is displaced toward an octahedral face, resulting in three short Nb–O contacts ($d < 1.95 \text{ \AA}$), each of which is *trans* to one of three long Nb–O bonds ($d > 2.05 \text{ \AA}$), compared to an expected Nb–O bond length of 1.99 Å on the basis of ionic radii data [$r(\text{Nb}^{5+}) = 0.78 \text{ \AA}$, $r(\text{O}^{2-}) = 1.21 \text{ \AA}$].¹⁸ The magnitude of the octahedral distortion, Δ_{Oct} of 0.203 Å in $\text{Na}_{1/2}(\text{H}_3\text{O})_{1/2}\text{Nb}_2\text{PO}_8$ is compatible to that observed in the two distinct TiO_6 octahedra in KTP-type materials: For KTiOPO_4 , $\Delta_{\text{Oct}}[\text{Ti}(1)] = 0.229 \text{ \AA}$ and $\Delta_{\text{Oct}}[\text{Ti}(2)] = 0.174 \text{ \AA}$.¹⁹ In KTiOPO_4 and its isomorphs, the TiO_6 distortion is almost exclusively along a Ti–O bond axis, leading to a situation where the central titanium atom makes one short, one long, and four “intermediate” bonds to oxygen, compared to the “three short/three long” situation in $\text{Na}_{1/2}(\text{H}_3\text{O})_{1/2}\text{Nb}_2\text{PO}_8$. The octahedral distortion in these “ Nb^{5+} ” and “ Ti^{4+} ” species with (formal) d^0 electron configurations may be interpreted in terms of a second-order Jahn–Teller effect.²⁰

Of the three cations which occupy “extra-framework” sites, Na(1), whose fractional site occupancy factor is unity, is six-coordinate to oxygen and occupies the cavity at the center of the cell [$(\frac{1}{2}, \frac{1}{2}, \frac{1}{2})$ site], with six equivalent Na(1)–O(1) contacts of 2.498(5) Å, in squashed trigonal-prismatic (site symmetry 32) configuration, as shown in Figure 4. The Na(2) and O(6) sites, the latter being part of a H_3O^+ hydronium ion, are located in the one-dimensional channels. These atomic species were initially assigned to their Fourier-map electron density maxima on the basis of bond/distance angle criteria (see Table III). Assuming O(6) to be part of a water molecule did not fulfill the requirement for charge-balancing the anionic framework, thus the oxygen atom of a hydronium species was subsequently assumed to occupy this site. Greater

(18) Shannon, R. D. *Acta Crystallogr.* 1976, A32, 751.

(19) Crystal data taken from: Thomas, P. A.; Glazer, A. M.; Watts, B. E. *Acta Crystallogr.* 1990, B46, 333.

(20) Phillips, M. L. F.; Harrison, W. T. A.; Grier, T. E.; Stucky, G. D.; Kulkarni, G. V.; Burdett, J. K. *Inorg. Chem.* 1990, 29, 2158.

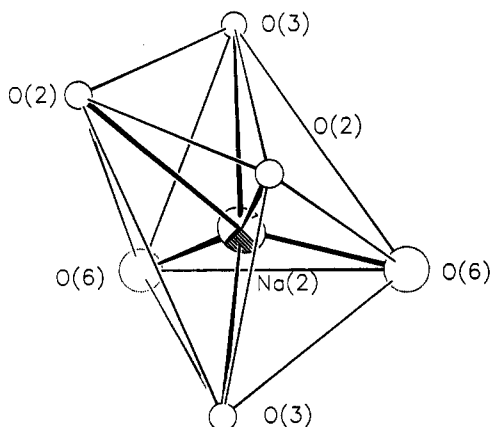


Figure 5. Na(2) coordination in $\text{Na}_{1/2}(\text{H}_3\text{O})_{1/2}\text{Nb}_2\text{PO}_8$ showing its pseudo-octahedral geometry. The O(6) atoms outlined with dotted lines are disordered. O...O contacts <4.2 Å are indicated by thin lines.

than 50% occupancy for both the channel sites at the same time is precluded by an unreasonable Na(2)...O(6) contact (~ 2.0 Å), and thus the initial occupancies were each set to 33% (the charge-balancing criterion) and allowed to refine to the final values shown in Table II, subject to the constraint of $\Delta f[\text{Na}(2)] = -\Delta f[\text{O}(6)]$ (f = fractional site occupancy). This constraint also allowed physically reasonable anisotropic thermal factors to be refined for each site. The U_{ij} values for both Na(2) and O(6) indicate some disorder in the channel direction, however. Attempts to refine other models based on a different distribution of atomic species invariably led to nonphysical thermal parameters and poorer R factors. However, the presence of some water, as opposed to hydronium cations, on the O(6) site cannot be completely ruled out: for instance one or more of the framework oxygen atoms may be (partially) protonated. Na(2) occupies a four-coordinate site at the side of the one-dimensional channel, and its coordination approximates an octahedron with two *cis* vertexes removed. These two vertexes are "occupied" by the guest hydronium cation (Figure 5); however, the apparent Na(2)–O(6) distance is very short, precluding simultaneous Na(2)/O(6) occupation of adjacent sites. O(6) bonds to seven distinct framework-oxygen species, with two possible H-bond connections to O(2) [$d(\text{O}(6)\cdots\text{O}(2)) = 2.95(1)$ Å \times 2]. O(6)'s unusual coordination is approximately heptagonal coplanar (Figure 6). Interestingly, the refined site-occupancy factors for the extra-framework species lead to a stoichiometry of almost exactly $\text{Na}_{1/2}(\text{H}_3\text{O})_{1/2}\text{Nb}_2\text{PO}_8$ ($\text{Na}_{0.5003}(\text{H}_3\text{O})_{0.4997}\text{Nb}_2\text{PO}_8$), and the compound is hereafter referred to as such.

^{31}P MAS NMR. The ^{31}P magic angle spinning NMR spectrum of $\text{K}_{2/3}\text{Li}_{1/3}\text{Nb}_2\text{PO}_8$ shows a single broad peak centered at $+6.7$ ppm, which we denote as site P(1). This is consistent with the structural refinement in that there is only one crystallographically unique phosphorus-atom site per asymmetric unit. The broadening of the peak may be due to three reasons: First, dipole–dipole coupling of ^{31}P to ^{93}Nb , which is a quadrupolar nucleus with spin $I = 9/2$ and a quadrupole moment of -0.2×10^{-24} cm 2 . Second, we believe that crystallographic disorder of the K^+ and Li^+ guest species may result in different local environments for the P-atom species. This effect is presently being investigated further. A third contribution to peak broadening may arise from the reversible absorption of water as described below.

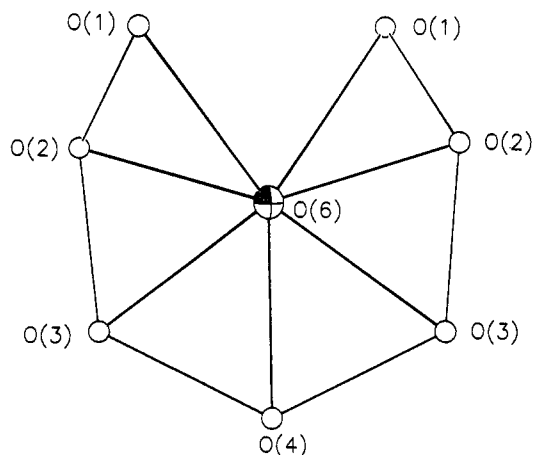


Figure 6. Hydronium ion [O(6)] coordination in $\text{Na}_{1/2}(\text{H}_3\text{O})_{1/2}\text{Nb}_2\text{PO}_8$, showing its almost planar 7-fold coordination.

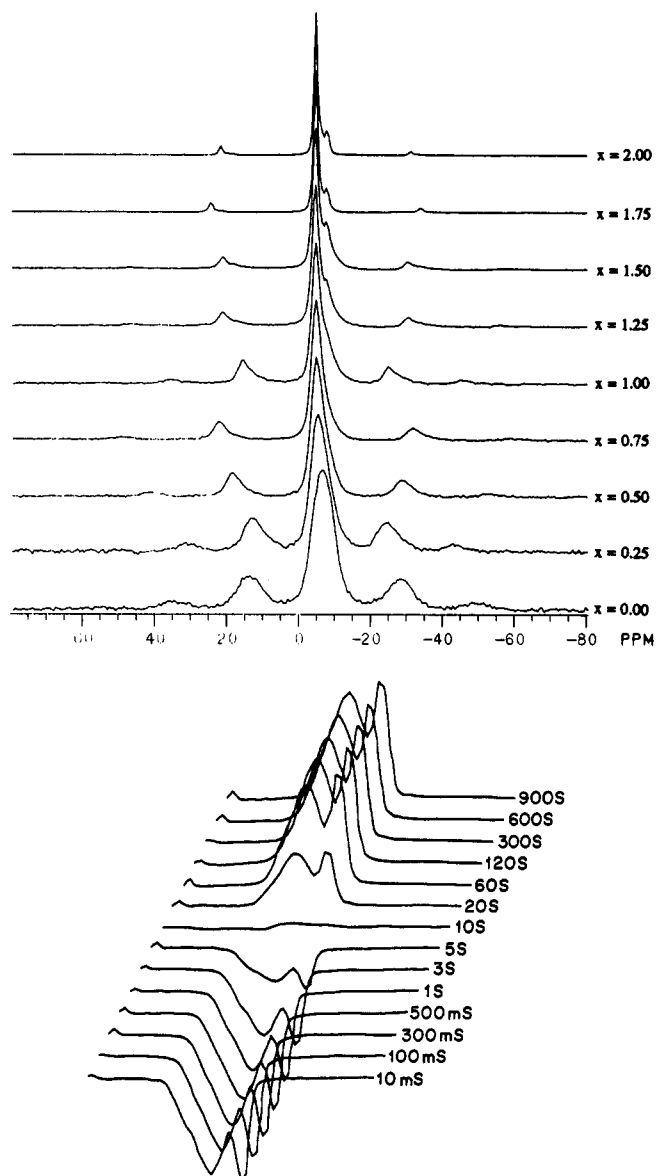


Figure 7. (a, top) "stacked plot" of ^{31}P MAS NMR spectra for the $\text{K}_{2/3}\text{Li}_{1/3}\text{Nb}_{2-x}\text{Ta}_x\text{PO}_8$ series. (b, bottom) Plot of inversion recovery (TIIR) system.

Figure 7a shows that the ^{31}P MAS NMR isotropic chemical shifts for the P-atom resonance, P(1), shifts downfield from -6.7 to -5.4 ppm upon doping the system

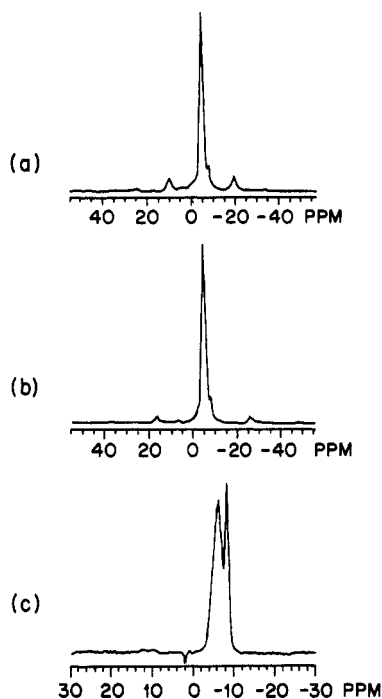


Figure 8. ^{31}P MAS NMR spectra of (a) newly synthesized $\text{K}_{2/3}\text{Li}_{1/3}\text{Ta}_2\text{PO}_8$ after heating at 1000°C and exposure to air for 3 h; (b) $\text{K}_{2/3}\text{Li}_{1/3}\text{Ta}_2\text{PO}_8$ annealed at 800°C in oxygen, and exposed to air for 24 h; (c) the same sample after exposure to air for 1 year.

with 12.5 atom % tantalum ($x = 0.25$ for $\text{K}_{2/3}\text{Li}_{1/3}\text{Nb}_{2-x}\text{Ta}_x\text{PO}_8$), and a new phosphorus atom resonance, P(2), at around -7 ppm appears as an upfield shoulder which becomes more apparent as the tantalum concentration increases to 62.5% ($x = 1.25$). From this figure, we are able to observe two trends above 62.5% tantalum doping: first, the shoulder becomes more pronounced as the Ta doping-level increases, and second, there is a decrease in line width. Finally, at 100% tantalum substitution ($\text{K}_{2/3}\text{Li}_{1/3}\text{Ta}_2\text{PO}_8$), there is a distinct second peak which appears upfield to P(1) at -7.9 ppm.

To eliminate the possibility that the second resonance was due to an impurity phase or amorphous material, the inversion-recovery experiment was carried out for $\text{K}_{2/3}\text{Li}_{1/3}\text{Ta}_2\text{PO}_8$, as described above (Figure 7b). The two resonances [P(1) and P(2)] show identical T_1 's, indicating that these two observed resonances are due to P atoms from the same phase, thus indicating this polycrystalline material is pure, and there is no amorphous material present. The T_1 for this material was calculated to be $15.22(6)$ μs .

Since there is only one crystallographically unique phosphorus atom present, there should be only one observable ^{31}P isotropic chemical shift. We believe that the second peak observable in the Ta-rich systems is due to the interaction between the framework phosphorus atoms and absorbed water molecules present in the extra-framework channels. This effect is presumably prevalent for the entire solid solution studied, but in the niobium-rich compounds the upfield peak is hidden by the line-broadening effects described above.

Figure 8 shows the following ^{31}P MAS NMR spectra: (a) the newly synthesized $\text{K}_{2/3}\text{Li}_{1/3}\text{Ta}_2\text{PO}_8$ after heating at 1000°C , and exposure to air for 3 h; (b) the same sample annealed at 800°C in oxygen, and exposed to air for 24 h; (c) the same sample after remaining in air for 1 year. From these data we propose that the second resonance

Table IV. Physical Data for $\text{K}_{2/3}\text{Li}_{1/3}\text{Nb}_{2-x}\text{Ta}_x\text{PO}_8$ Series^a

	a (Å)	c (Å)	V (Å ³)	SHG ^b	edge ^c	$^{31}\text{P}_{iso}$
$\text{K}_{2/3}\text{Li}_{1/3}\text{Nb}_2\text{PO}_8$	13.095	10.242	1583	106	365	-6.7
$\text{K}_{2/3}\text{Li}_{1/3}\text{Nb}_{1.75}\text{Ta}_{0.25}\text{PO}_8$	13.187	10.386	1579	117	360	-5.4
$\text{K}_{2/3}\text{Li}_{1/3}\text{Nb}_{1.50}\text{Ta}_{0.50}\text{PO}_8$	13.239	10.397	1582	108	350	-5.0
$\text{K}_{2/3}\text{Li}_{1/3}\text{Nb}_{1.33}\text{Ta}_{0.67}\text{PO}_8$	13.237	10.389	1577	97		
$\text{K}_{2/3}\text{Li}_{1/3}\text{Nb}_{1.25}\text{Ta}_{0.75}\text{PO}_8$	13.241	10.399	1580	104	347	-4.9
$\text{K}_{2/3}\text{Li}_{1/3}\text{Nb}_{1.00}\text{Ta}_{1.00}\text{PO}_8$	13.241	10.393	1578	86	344	-4.9
$\text{K}_{2/3}\text{Li}_{1/3}\text{Nb}_{0.75}\text{Ta}_{1.25}\text{PO}_8$	13.231	10.396	1576	74	335	-4.8
$\text{K}_{2/3}\text{Li}_{1/3}\text{Nb}_{0.67}\text{Ta}_{1.33}\text{PO}_8$	13.233	10.384	1575	82		
$\text{K}_{2/3}\text{Li}_{1/3}\text{Nb}_{0.50}\text{Ta}_{1.50}\text{PO}_8$	13.247	10.390	1579	68	330	-4.8
$\text{K}_{2/3}\text{Li}_{1/3}\text{Nb}_{0.38}\text{Ta}_{1.62}\text{PO}_8$	13.237	10.402	1578	77		
$\text{K}_{2/3}\text{Li}_{1/3}\text{Nb}_{0.25}\text{Ta}_{1.75}\text{PO}_8$	13.234	10.394	1576	91	323	-4.9
$\text{K}_{2/3}\text{Li}_{1/3}\text{Nb}_{0.13}\text{Ta}_{1.87}\text{PO}_8$	13.243	10.407	1581	88		
$\text{K}_{2/3}\text{Li}_{1/3}\text{Ta}_2\text{PO}_8$	13.237	10.384	1572	74	297	-4.9

^a Estimated errors: a (± 0.005 Å), c (± 0.005 Å), V (± 2 Å³), SHG ($\pm 10\%$), edge (± 2 nm), $^{31}\text{P}_{iso}$ resonance (± 2 ppm). The transformation between hexagonal and rhombohedral settings of the $\text{Na}_{1/2}(\text{H}_3\text{O})_{1/2}\text{Nb}_2\text{PO}_8$ -type unit cell is effected by the transformation matrix given in ref 23. ^b Relative to quartz. ^c Inflection point of absorption edge in nanometers (see text).

observable in the Ta-containing system may be due to the interaction of framework P atoms with guest water molecules sorbed into the extra-framework channels.

These NMR data may be compared with a TGA measurement on a sample of $\text{K}_{2/3}\text{Li}_{1/3}\text{Nb}_2\text{PO}_8$ exposed to air for several months, which shows that there is 2.99% weight loss at 100°C and a second weight loss of $\sim 0.76\%$ at around 350°C . X-ray data recorded at the end of the TGA run show that the material maintained its rhombohedral structure.

Optical Responses. In general, these compounds are yellow at high temperatures and slowly turn almost colorless as they cool (we have noted that the higher the niobium content, the darker the high-temperature color). Data on SHF, UV/vis spectra, ^{31}P MAS NMR, and X-ray powder diffraction are collated for each compound in the $\text{K}_{2/3}\text{Li}_{1/3}\text{Nb}_{2-x}\text{Ta}_x\text{PO}_8$ series in Table IV. During initial tests, we found that these compounds were easily damaged by the laser during the SHG studies, which we attribute to the presence of oxygen atom defects in the (Nb,Ta)/P/O framework. A similar phenomenon has also been observed in lithium niobate, where oxygen defects give LiNbO_3 its light yellow color.¹⁷ Accordingly, each compound was heated to 850°C for 24 h in flowing oxygen, and fast-quenched to room temperature by removing the quartz boat from the hot-tube furnace to an aluminum plate. X-ray powder diffraction data show a slight decrease in cell volume for the oxygen-annealed samples.

SHG measurements of the oxygen-treated samples (Table IV) did not reveal any significant laser damage. For hydrothermally grown single crystals of $\text{Na}_{1/2}(\text{H}_3\text{O})_{1/2}\text{Nb}_2\text{PO}_8$ and $\text{Na}_{1-x}(\text{H}_3\text{O})_x\text{Ta}_2\text{PO}_8$, the SHG intensities were collected on ground-up crystals. These samples gave somewhat lower SHG values (Table V) than the corresponding solid-state synthesized samples (Table IV). The SHG values of more than $100 \times$ quartz are relatively large and comparable to those of polycrystalline $\beta\text{-BaB}_2\text{O}_4$ ($82 \times$ quartz) for a Nd:YAG 1064-nm primary beam.²¹

Vis/UV data (Table IV) show that as the atom percentage of Ta increases, the absorption edge shifts toward higher energy. The absorption edge for $\text{K}_{2/3}\text{Li}_{1/3}\text{Nb}_2\text{PO}_8$ is $360(2)$ nm, which shows a systematic shift with Ta-

(21) SHG data for polycrystalline $\beta\text{-BaB}_2\text{O}_4$ supplied by J. D. Bierlein, Central Research and Development Laboratory, E. I. du Pont de Nemours, Wilmington, DE.

Table V. Physical Data for $M(\text{Nb,Ta})_2\text{PO}_8$ Phases^a

composition	<i>a</i> (Å)	<i>c</i> (Å)	<i>V</i> (Å ³)	SHG ^b	edge ^c	³¹ P _{iso}
Na _{2/3} Li _{1/3} Nb ₂ PO ₈	13.362	10.299	1593	42	320	<i>d</i>
Rb _{2/3} Li _{1/3} Nb ₂ PO ₈	13.283	10.381	1586	97	328	-5.7
Na _{1-x} (H ₃ O) _x Ta ₂ PO ₈	13.470	10.303	1619	40	320	<i>d</i>
Na _{1-x} (H ₃ O) _x Ta ₂ PO ₈	13.425	10.318	1611	40	300	-6.6
Rb _{2/3} Li _{1/3} Nb ₂ PO ₈	13.283	10.381	1586	97	328	-5.7
K _{2/3} Ag _{1/3} Nb ₂ PO ₈	13.456	10.319	1618	26	428	-4.6
(NH ₄) _{2/3} Li _{1/3} Nb ₂ PO ₈	13.144	10.477	1567	109	326	-5.5/-6.8

^a Estimated errors: *a* (± 0.005 Å), *c* (± 0.004 Å), *V* (± 2 Å³), SHG ($\pm 10\%$), edge (± 2 nm). ³¹P_{iso} resonance (± 0.2 ppm). ^b Relative to quartz. ^c Inflection point of absorption edge in nanometers (see text). ^d Multiple ³¹P resonances observed (see text).

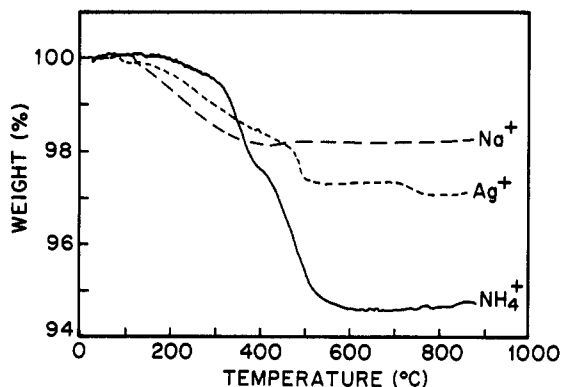


Figure 9. TGA traces for various ion-exchanged $\text{K}_{2/3}\text{-Li}_{1/3}\text{-Nb}_2\text{PO}_8$ -type phases.

atom doping to 297(2) nm for $\text{K}_{2/3}\text{Li}_{1/3}\text{Ta}_2\text{PO}_8$. Since a fixed-wavelength laser (Nd:YAG, 1064 nm) was used to collect all SHG data, the greater difference between the excitation frequency and the absorption edge is expected to lead to smaller SHG values for the Ta-rich phases. This is consistent with the data which show a decrease in SHG intensity (from 106 to 74 \times quartz for $\text{K}_{2/3}\text{Li}_{1/3}\text{Nb}_2\text{PO}_8$ and $\text{K}_{2/3}\text{Li}_{1/3}\text{Ta}_2\text{PO}_8$, respectively).

TGA/Ion-Exchange Studies. TGA (Figure 9) of $\text{K}_{2/3}\text{Li}_{1/3}\text{Nb}_2\text{PO}_8$ and X-ray data recorded after the TGA run shows that the structure is maintained on thermal treatment. However, for the hydronium-containing compounds, the loss of water results in the collapse of the structure. For example, the TGA data for $\text{Na}_{1-x}(\text{H}_3\text{O})_x\text{Ta}_2\text{PO}_8$, show a 4.18% weight loss equivalent to a loss of ~ 0.85 of a water molecule. The powder pattern of the post-TGA residue of $\text{Na}_{1-x}(\text{H}_3\text{O})_x\text{Ta}_2\text{PO}_8$ indicated a new crystalline material of unknown structure.

The weight-change monitored by careful weighing of the sample before and after ion exchange, confirmed that when $\text{K}_{2/3}\text{Li}_{1/3}\text{Nb}_2\text{PO}_8$ was treated with NH_4NO_3 , as described above, 97% of NH_4^+ was exchanged for K^+ , giving $\sim (\text{NH}_4)_{2/3}\text{Li}_{1/3}\text{Nb}_2\text{PO}_8$ as the product. The unit-cell volume of the material after ammonium exchange decreased from 1583(1) Å³ to 1567(3) Å³. An IR spectrum of the NH_4^+ -exchanged product (Figure 10) shows a peak at 1427 cm^{-1} which is characteristic of N-H bending, and peaks at 3047 and 3258 cm^{-1} which correspond to N-H stretching frequencies.

Upon ion exchange of NH_4^+ for K^+ , the optical absorption edge is shifted from 365(2) nm to 326(2) nm (Table V). On deammoniation there is a 5.4% weight loss, and X-ray diffraction of the deammoniated material indicated the presence of a new, unknown phase. The ³¹P MAS NMR spectrum of the $(\text{NH}_4)_{2/3}\text{Li}_{1/3}\text{Nb}_2\text{PO}_8$ sample reveals two isotropic chemical shifts (-5.5 and -6.8 ppm), which

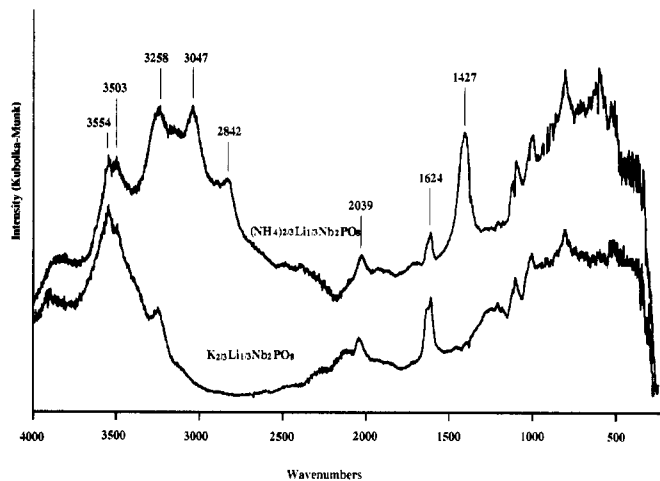


Figure 10. IR spectrum of (a) $\text{K}_{2/3}\text{Li}_{1/3}\text{Nb}_2\text{PO}_8$ and (b) of the same material after NH_4^+ exchange.

may be due to inequivalent framework P atom-guest NH_4 molecule interactions. A single ¹H MAS NMR isotropic chemical shift is found for $(\text{NH}_4)_{2/3}\text{Li}_{1/3}\text{Nb}_2\text{PO}_8$ at +7.1 ppm, a typical value for ammonium group protons, offering further evidence that that NH_4^+ has been successfully incorporated into the channels.

For sodium exchange into $\text{K}_{2/3}\text{Li}_{1/3}\text{Nb}_2\text{PO}_8$, weight-change data indicate $\sim 50\%$ exchange of Na^+ , relative to K^+ , and X-ray powder diffraction data confirms the existence of a single-phase product, with narrow line widths. ³¹P MAS NMR isotropic chemical shift shows that there is only one unique phosphorus atom site for the ion-exchanged compounds (see Table V). For sodium-exchanged $\text{K}_{2/3}\text{Li}_{1/3}\text{Nb}_2\text{PO}_8$, unit-cell volume is 1601(1) Å³, an increase of 1.14% relative to the unexchanged material. The absorption edge obtained from UV/VIS data is at 326(2) nm (Table V).

$\text{K}_{2/3}\text{Ag}_{1/3}\text{Nb}_2\text{PO}_8$ ($>90\%$ exchange of Ag^+ for Li^+ by weight-change measurements) is yellow and light sensitive. The powder X-ray data for $\text{K}_{2/3}\text{Ag}_{1/3}\text{Nb}_2\text{PO}_8$ indicate a rhombohedral unit-cell with a volume of 1618(1) Å³. ³¹P isotropic chemical shift data reveal one magnetically unique phosphorus atom which appears downfield from $\text{K}_{2/3}\text{Li}_{1/3}\text{Nb}_2\text{PO}_8$, at -4.6 ppm. The UV/vis data collected on newly exchanged $\text{K}_{2/3}\text{Ag}_{1/3}\text{Nb}_2\text{PO}_8$ show an absorption edge of 428(2) nm. The SHG intensities for Ag^+ -exchanged $\text{K}_{2/3}\text{Li}_{1/3}\text{Nb}_2\text{PO}_8$ decrease from 106 to 26 \times quartz (Table V). This phenomenon of decreasing SHG response has also been observed in silver-exchanged KTP, and a mechanism involving strong guest Ag-framework O bonding may be responsible.²² The TGA data for $\text{K}_{2/3}\text{-Ag}_{1/3}\text{Nb}_2\text{PO}_8$ show an initial weight loss of 1.9% at 100 °C, a second weight loss of 0.7% at 472 °C, and a further weight loss of 0.2% around 700 °C.

X-ray powder diffraction data of $\text{K}_{2/3}\text{Ag}_{1/3}\text{Nb}_2\text{PO}_8$ heated to 475 °C for 20 h illustrates that the compound maintains its rhombohedral structure, but after heating to 700 °C, a new material of unknown structure results. This phase change could be attributed to the fact that the silver migrates to the outside of the channels thus resulting in the collapse of the open framework, a phenomenon which has been observed for many silver-exchanged zeolitic

(22) Phillips, M. L. F.; Harrison, W. T. A.; Gier, T. E.; McCarron III, E. M.; Calabrese, J. C.; Stucky, G. D. *Chem. Mater.* 1992, 4, 222.

(23) Arnold, H. *International Tables for X-Ray Crystallography*; Kluwer Academic Publishers: Dordrecht, 1992; Volume A, Table 5.1.

materials. Attempts have been made to exchange Rb^+ for K^+ by heating excess RbNO_3 with $\text{K}_{2/3}\text{Li}_{1/3}\text{Nb}_2\text{PO}_8$ to 225°C for 1 week. Weight-change measurements indicated that the degree of ion-exchange was negligible, perhaps due to cation size differences. However, K^+ may be successfully exchanged into $\text{Rb}_{2/3}\text{Li}_{1/3}\text{Nb}_2\text{PO}_8$ via a KNO_3 melt.

Conclusion

Members of a new class of ion-exchangeable, open-framework nonlinear optical materials have been prepared and the structure of hydrothermally grown $\text{Na}_{1/2}(\text{H}_3\text{O})_{1/2}\text{Nb}_2\text{PO}_8$ has been characterized by single-crystal X-ray diffraction. The complete solid solution $\text{K}_{2/3}\text{Li}_{1/3}\text{Nb}_{2-x}\text{Ta}_x\text{PO}_8$ ($0 < x < 2$) is accessible via solid-state preparation methods.

SHG measurements for the polycrystalline $\text{K}_{2/3}\text{Li}_{1/3}\text{Nb}_{2-x}\text{Ta}_x\text{PO}_8$ series indicate that all compositions are noncentrosymmetric with SHG values relative to quartz compatible to that found for $\beta\text{-BaB}_2\text{O}_4$. UV/visible data show that the absorption edge shifts regularly from 360 to 297 nm with increasing Ta composition. We have

discovered several ion-exchange processes which appear to be (Na/Li/K) cation specific, on the basis of weight-change measurements. ^{31}P MAS NMR isotropic chemical shift data demonstrate both the effect of water intercalation in the extra-framework channels and the dipole-dipole coupling between ^{31}P and the quadrupolar ^{93}Nb nuclei.

The ability for ion exchange in these phases leads to possibilities for this material other than a frequency doubler, e.g., as a waveguide for optical transmission or optical switching. The crystal structures of several of these ion-exchanged materials are now being investigated.

Acknowledgment. We are grateful to Dr. Helmut Eckert (UCSB) for helpful suggestions regarding the NMR studies and Dr. Vojislav Srdanov (UCSB) for setting up the SHG apparatus. This work is supported by the National Science Foundation, Grant DMR 9208511.

Supplementary Material Available: Tables of anisotropic thermal factors (1 page); final observed and calculated structure factor amplitudes (4 pages). Ordering information is given on any current masthead page.